HHS Public Access

Author manuscript

Clin Pharmacol Ther. Author manuscript; available in PMC 2022 February 01.

Published in final edited form as:

Clin Pharmacol Ther. 2021 February ; 109(2): 494–506. doi:10.1002/cpt.2021.

Physiologically Based Pharmacokinetic Modeling of Central Nervous System Pharmacokinetics of CDK4/6 Inhibitors to Guide Selection of Drug and Dosing Regimen for Brain Cancer Treatment

Jing Li[1,*], **Jun Jiang**[1], **Jianmei Wu**[1], **Xun Bao**[1], **Nader Sanai**[2]

[1]Karmanos Cancer Institute, Wayne State University School of Medicine, Detroit, MI 482012

[2]Barrow Neurological Institute, St. Joseph's Hospital & Medical Center, Phoenix, AZ 85013

Abstract

A better understanding of the human central nervous system (CNS) pharmacokinetics is critical to the selection of the right drug and refinement of dosing regimen for more effective treatment of primary and metastatic brain cancer. Using the physiologically based pharmacokinetic (PBPK) modeling approach, we systematically compared the CNS pharmacokinetics of three CDK4/6 inhibitors (ribociclib, palbociclib, and abemaciclib) in cancer patients. A PBPK model platform was developed and verified for predicting plasma and CNS pharmacokinetics. Target engagement ratio (TER), defined as the ratio of the average steady-state unbound drug brain concentration to the *in vitro* IC_{50} for CDK4/6 inhibition, was used as a crude predictor of efficacy. As compared to ribociclib and palbociclib, abemaciclib penetrated into the human brain to a larger extent, but at a slower rate, and retained in the brain longer. Following the standard dosing regimens, the predicted CDK4/6 TERs were 26/5.2 for abemaciclib, 2.4/0.62 for ribociclib, and 0.36/0.27 for palbociclib. Simulations suggested that abemaciclib achieved comparable TERs following twice daily or daily dosing; ribociclib may sufficiently inhibit both CDK4 and CDK6 at the maximum tolerated dose; whereas, palbociclib achieved TERs < 0.5 even at a dose 50% higher than the standard dose. In conclusion, the PBPK modeling, supported by available preclinical and clinical evidence, suggests that abemaciclib is the best CDK4/6 inhibitor for brain cancer treatment, while palbociclib is not recommended. The model refined dosing regimen is 300 mg daily on a 4-weeks-on schedule for abemaciclib, and 900 mg daily on a 3-weeks-on/1-week-off schedule for ribociclib.

Keywords

physiologically based pharmacokinetic (PBPK) model; central nervous system pharmacokinetics; ribociclib; palbociclib; abemaciclib; brain cancer

[*]**Corresponding authors:** Jing Li, Ph.D., Karmanos Cancer Institute, 4100 John R Street, HWCRC, Room 523, Detroit, MI 48201, USA; Phone: 313-576-8258; LiJing@wayne.edu.

Author contributions

J.L. wrote the manuscript; J.L. designed the research; J.L., J.J., J.W., X.B., and N.S. performed the research; J.L. analyzed the data.

Conflict of Interest: The authors declared no competing interests for this work.

INTRODUCTION

Despite significant advances in understanding cancer biology, the mortality rates for primary and metastatic brain cancer have remained steady for more than 30 years. For patients with newly diagnosed glioblastoma (the most common and aggressive malignant primary brain cancer), the median overall survival is 14.6 months with the current standard of care.[1,2] For patients with metastatic brain cancer, occurring in 10–35% of adult patients with non-brain primary cancer,[3] the median overall survival is 7.2 months.[4] There is an unmet need for the development of more effective drug therapies for both primary and metastatic brain cancer.

Loss of cell cycle regulation leading to uncontrolled cellular proliferation is a hallmark of cancer. The cyclin D-cyclin dependent kinase 4 and 6 (CDK4/6)-retinoblastoma (Rb) pathway is a key regulator of cell cycle, where CDK4/6 interact with cyclin D to phosphorylates the tumor suppressor protein Rb and subsequently release the transcription factor E2F, thus promoting the G1 to S phase cell cycle progression. The cyclin D-CDK4/6-Rb pathway is often dysregulated in virtually all human cancers via both genetic and epigenetic mechanisms, resulting in increased kinase activity.[5–7] Excessive CDK4/6 activity may suppress senescence and directly contribute to both initiation and maintenance of cell transformed state.[8,9] Inhibition of the cyclin D-kinase activity has emerged as a novel cancer therapeutic strategy. Three orally bioavailable, selective, small molecule CDK4/6 inhibitors including ribociclib, palbociclib, and abemaciclib have been approved by the United States Food and Drug Administration (FDA) as monotherapy or combination with hormone therapy for treating hormone receptor-positive, HER2-negative metastatic breast cancers.[10] In light of the central role of the cyclin D-CDK4/6-Rb pathway in controlling cellular proliferation and its frequent dysregulation in glioblastoma and cancers with a high incidence of brain metastases, CDK4/6 inhibitors are currently under active clinical investigation in patients with glioblastoma[11,12] and brain metastases of breast cancer, non-small cell lung cancer, or melanoma (ClinicalTrials.gov Identifier: NCT02308020).

While sharing a similar mechanism of action, ribociclib, palbociclib, and abemaciclib are distinct with respect to physicochemical properties, selectivity and potency for CDK4/6 inhibition, pharmacokinetics, and clinical toxicity profiles.[13,14] In addition, preclinical studies and preliminary clinical data suggest that the three CDK4/6 inhibitors plausibly penetrate into the human central nervous system (CNS) to a different extent.[12,14–16] Sufficient drug penetration into brain tumors, particularly into the invasive, infiltrating tumor cells behind an intact blood-brain barrier (BBB), is the prerequisite for consistent *in vivo* target inhibition and efficacious treatment of primary brain cancer or brain metastasis.[17] Selection of the CDK4/6 inhibitor(s) with favorable CNS pharmacokinetics and design of optimal dosing regimen will maximize the success in the development of these novel agents for brain cancer treatment. However, as many other new or existing anticancer drugs, the CNS pharmacokinetics of the three CDK4/6 inhibitors in cancer patients remain understudied and poorly understood largely due to the difficulty to accessing human brain tissues and the lack of *in vitro* or animal models that reliably predict human BBB permeability. Therefore, it is imperative that innovative approaches are developed to more reliably predict drug disposition in the human CNS. One such an approach is the *in vitro-in vivo* extrapolation, physiologically based pharmacokinetic (IVIVE-PBPK) modeling that

enables prediction of pharmacokinetic processes in the system and individual organs by integrating human physiological parameters (e.g., enzyme and transporter protein abundances in organs) with drug-specific parameters (e.g., physicochemical properties, *in vitro* metabolism and transporter kinetics).[18]

In this study, we developed and verified a whole-body PBPK model integrated with a 4-compartment permeability-limited brain model platform that accounted for the general anatomical structure of the human CNS and key processes governing the CNS pharmacokinetics of a drug. This mechanism-based model platform allowed prediction of the plasma and CNS pharmacokinetics of CDK4/6 inhibitors following various dosing regimens. Our study provided critical mechanistic and quantitative information to guide selection of the right drug and refinement of dosing regimen for the rational development and optimal use of CDK4/6 inhibitors for brain cancer treatment.

METHODS

In vitro studies

In vitro studies were performed to determine drug-specific parameters for ribociclib, palbociclib, and abemaciclib, including *in vitro* metabolic intrinsic clearance by human liver and intestinal microsomes, fraction unbound in patient plasma and brain tumor tissues, apparent transcellular passive permeability, and ABCB1/ABCG2-mediated intrinsic efflux clearance. Details for *in vitro* experiments are provided in Supplementary Materials.

PBPK modeling and simulation

PBPK model development—A whole-body PBPK model integrated with a 4Brain model (Figure 1) was developed for predicting the system and CNS pharmacokinetics of each CDK4/6 inhibitor, using the Simcyp Simulator® V18 (Simcyp Ltd, Sheffield, United Kingdom). System-specific parameters were derived from the existing Simcyp virtual cancer patient population, unless stated otherwise. Drug-specific parameters are summarized in Table 1. The model development was described in details in Supplementary Materials.

Model verification—The total and unbound drug concentration – time profiles of each CDK4/6 inhibitor in the plasma, brain, and CSF were predicted in a Simcyp virtual cancer population by simulations of 10 trials with 10 subjects in each trial. The dosing regimens for simulations were matched to the FDA-approved standard dose regimens or that used in the published clinical trials. The developed PBPK models were verified by comparing the model-predicted plasma and CNS pharmacokinetics with the observed clinical plasma and CNS (if available) data.

Simulations—To assist the design of optimal dosing regimens, simulations of 10 trials with 10 cancer patients in each trial were performed to predict the plasma and CNS pharmacokinetics of each CDK4/6 inhibitor following the FDA-approved standard and modified dosing regimens. The standard dosing regimen for ribociclib is 600 mg once daily (QD) oral dosing on a 3-weeks-on/1-week-off schedule; for palbociclib is 125 mg QD oral dosing on a 3-weeks-on/1-week-off schedule; and for abemaciclib is 150 mg twice daily

(BID) oral dosing on a 4-weeks-on continuous schedule. Modified dosing evaluated were 900 mg QD (maximum tolerated dose) for ribociclib, 187.5 mg QD (50% increase of the standard dose) for palbociclib, and 300 mg QD for abemaciclib.

RESULTS

Drug-specific parameters

In vitro metabolic kinetics—The overall metabolic kinetics of ribociclib, palbociclib, and abemaciclib in human liver and intestinal microsomes were well described by Michaelis-Menten kinetics (Figure S1). The estimated *in vitro* metabolic kinetic parameters, including the maximum metabolic velocity (V_{max}), substrate concentration at which 50% of V_{max} is obtained (K_m), and *in vitro* intrinsic metabolic clearance (CL_{int}) estimated as V_{max}/K_m, are summarized in Table 1 and were used for predicting the whole-organ liver and intestine metabolic clearance in the PBPK models.

Binding to patient plasma proteins and brain tumor tissues—In cancer patient plasma, ribociclib and palbociclib were bound to plasma proteins to a similar extent, with the mean fraction unbound in plasma ($f_{u,p}$) 0.125 and 0.126, respectively, while abemaciclib had higher plasma binding (mean $f_{u,p,}$ 0.06). Similarly, abemaciclib showed the highest binding to human brain tumor tissues with the mean fraction unbound in brain tissue ($f_{u,br}$) 0.006, followed by palbociclib (mean $f_{u,b}$, 0.015) and ribociclib (mean $f_{u,br}$, 0.044).

Passive transcellular permeability—The three CDK4/6 inhibitors exhibited similar apical-to-basolateral apparent transcellular passive permeability ($P_{app,A\text{-}B}$) across MDCKII cell monolayers at pH 7.4 in both apical and basolateral chambers (Table 2). Based on pH partition theory (Henderson-Hasselbalch equation), the unionization efficiency (λ) at pH 7.4 for ribociclib (PK_a, 8.87), palbociclib (PK_a, 8.86), and abemaciclib (PK_a, 7.94) was estimated to be 0.033, 0.034, and 0.224, respectively. Because only unbound and unionized drugs pass through biological membranes, the intrinsic passive transcellular permeability ($P_{app,A\text{-}B}/\lambda$) for unionized drugs were estimated (Table 2), and were then scaled to human brain microvasculature surface area to predict the BBB passive permeability clearance (PSB) of the unbound and unionized drug in the PBPK model (Table 1).

The three CDK4/6 inhibitors are weak base drugs. Similar to AZD1775 (a weak base drug),[19] the three CDK4/6 inhibitors exhibited pH-dependent apparent permeability across the MDCKII, MDCKII-ABCB1, and MDCKII-ABCG2 cell monolayers (Figure 2). As the pH decreased (7.4, 7.0, 6.5, and 6.0) in the basolateral chamber (mimicking brain/brain tumor interstitium) while remaining the same (7.4) in the apical chamber (mimicking blood circulation), the apparent permeability increased in the apical-to-basolateral direction while decreasing in the basolateral-to-apical direction, overall resulting in reduced efflux ratios (Figure 2). This observation was in accordance with the pH partition theory. At a relatively acidic basolateral pH, the ionization of a weak base drug was increased, and as a result, the basolateral-to-apical permeability decreased and apical-to-basolateral permeability increased, thus leading to the trap of ionized drugs in the basolateral compartment.

ABCB1- and ABCG2-mediated intrinsic efflux clearance—MDCKII cells with stable expression of ABCB1 or ABCG2 were used to determine the interactions of CDK4/6 inhibitors with ABCB1 and ABCG2, two major efflux transporters that are expressed at the human BBB. The positive controls, loperamide (a typical ABCB1 substrate) and gefitinib (a typical ABCG2 substrate) exhibited a mean net efflux ratio of 6.11 and 8.86 on MDCKII-ABCB1 and MDCKII-ABCG2 cell monolayers, respectively, confirming the functional expression of ABCB1 and ABCG2 in these cellular models. All three CDK4/6 inhibitors were ABCB1 substrates, while ABCB1 efflux efficiency appeared the highest for ribociclib (net efflux ratio 10.5), followed by palbociclib (net efflux ratio 5.92) and abemaciclib (net efflux ratio 2.84) (Table 2). Palbociclib was a substrate of ABCG2 (net efflux ratio 2.64), but ribociclib and abemaciclib were not good substrates for ABCG2 (net efflux ratio 1.02 and 1.21 respectively) (Table 2). Based on the intrinsic transcellular passive permeability and net efflux ratio, *in vitro* ABCB1-mediated intrinsic efflux clearance was determined to be 4354, 5232, and 160 μL/min/mg for ribociclib, palbociclib, and abemaciclib, respectively, and the respective *in vitro* ABCG2 intrinsic efflux clearance was 0, 1716 and 18 μL/min/mg (Table 1). These values were then scaled by IVIVE strategy to predict *in vivo* ABCB1- and ABCG2-mediated efflux clearance at the BBB.

In vivo-in vitro relative activity factor (RAF) of ABCB1 and ABCG2—Quantitative proteomics analyses of 30 human normal brain and 47 glioblastoma samples suggest that the median protein abundances of ABCB1 and ABCG2 are 3.38 and 6.21 pmol/mg in human normal brain microvessels, respectively; and their respective levels are reduced to 0.14 and 1.69 pmol/mg in human glioblastoma microvessels.[20] In the cell membranes of MDCKII-ABCB1 and MDCKII-ABCG2 cell lines, ABCB1 and ABCG2 protein abundances are 10.3 and 13.2 pmol/mg, respectively.[20] The mean recovery of microvessels isolated from human normal brain and glioblastoma is 0.19 and 0.31 mg per gram tissue, respectively.[20] Based on these data and given an average brain weight of 1400 g, the RAF for ABCB1 and ABCG2 was determined to be 87.3 and 125.1 mg at the intact human BBB, respectively, while being 5.88 and 55.5 mg at the BBB in glioblastoma.

ABCB1 has been located at the apical (CSF facing) membrane of the blood-cranial CSF barrier, and therefore ABCB1-mediated active influx from the blood to cranial CSF was considered at the blood-cranial CSF barrier However, ABCB1 protein abundance data at this barrier is not available, and thus the RAF for ABCB1-mediated active influx clearance at the blood-CSF barrier was assigned and verified by the observed clinical CSF data of ribociclib.

PBPK modeling and simulations

Model verification for prediction of plasma pharmacokinetics—Following the dosing regimen (900 mg QD for 5 days) as used in the clinical trial, the PBPK model well predicted ribociclib mean plasma concentration time profiles and inter-individual variabilities, as demonstrated by > 98% of observed plasma concentration data falling within the 5^{th} and 95^{th} percentiles of the simulated population mean profile (Figure 3A). The model-simulated population mean maximum plasma concentration (C_{max}) and apparent oral clearance (CL/F) of ribociclib were 1.03- and 0.90-fold of the respective observed

parameters (i.e., predicted vs. observed C_{max}, 3.87 vs. 3.75 μmol/L; CL/F, 55.5 vs. 61.6 L/h).[12]

Similarly, the developed PBPK models well predicted the plasma pharmacokinetics of palbociclib and abemaciclib. The simulated population mean plasma pharmacokinetic parameters were within 0.90–1.15 fold of the respective parameters estimated by population pharmacokinetic modeling analysis of observed data in cancer patients.[21,22] Specifically, the predicted vs. observed palbociclib CL/F was 59.4 vs. 63.1 L/h, elimination half-life ($T_{1/2}$) was 30 vs. 29 h, apparent volume of distribution (V/F) was 2283 vs. 2342 L, and oral bioavailability (F) was 0.47 vs. 0.46. The predicted vs. observed abemaciclib CL/F was 35.9 vs. 36.0 L/h, $T_{1/2}$ was 22 vs. 20 h, V/F was 1041 vs. 1050 L, and F was 0.52 vs. 0.45.

Model verification for prediction of CNS pharmacokinetics—Given the availability of ribociclib CNS pharmacokinetic data (i.e., CSF and tumor concentrations) observed in glioblastoma patients,[12] the 4Brain model was first developed and verified for the prediction of CNS pharmacokinetics of ribociclib. The simulated ribociclib CSF concentrations were in line with observed CSF data in glioblastoma patients, with all except for one observed data falling within the 5th and 95th percentiles of the simulated population mean profile (Figure 3B). The model-predicted population mean CSF-to-unbound plasma ratio (CSF $K_{p,uu}$, 1.6) was 0.9-fold of the observed median CSF $K_{p,uu}$ (1.8) in 12 glioblastoma patients.[12]

The physical and biochemical barriers of the BBB in glioblastomas are often disrupted, as indicated by leaky tight junctions and loss or significant reduction in protein expression of major BBB efflux transporters.[20] It has been reported that the median protein abundances of ABCB1 and ABCG2 in glioblastoma microvessels are reduced to 3.7% and 35% of the normal levels, respectively.[20] In addition, electrode measurements of pH in human brain tumors are as low as 5.9 with a mean around 6.8; whereas, normal human brain maintains a pH at approximately 7.1 – 7.2.[23–25] As demonstrated by the *in vitro* pH-dependent apparent permeability data (Figure 2), the relative acidic tumor environment would be favorable to the tumor penetration and trap of weak base drugs, regardless whether they are the substrates of ABCB1/ABCG2. The regional pH difference in the normal brain and brain tumors may contribute to the heterogeneous brain/tumor distribution of CDK4/6 inhibitors. Therefore, to predict ribociclib concentrations in the human normal brain as well as in contrast non-enhancing and enhancing tumor regions of glioblastoma, different ABCB1/ABCG2 protein abundances at the BBB and varying brain pH were applied in the simulations following the dosing regimen used in the clinical trial (900 mg QD for 5 days) (Figure 3C–3F). In the normal brain with an intact BBB (i.e., brain pH 7.12, ABCB1 abundance 3.38 pmol/mg), the simulated population mean steady-state average concentration ($C_{ss,ave}$) of unbound ribociclib was 0.036 μmol/L and unbound brain-to-plasma ratio ($K_{p,uu}$) was 0.14 (Figure 3C). In brain tumors with increasing BBB disruption, specifically in brain tumors with 1) pH 6.8 and ABCB1 abundance 0.14 pmol/mg (Figure 3D), 2) pH 6.8 and loss of ABCB1 expression (Figure 3E), and 3) pH 6.5 and loss of ABCB1 expression (Figure 3F), the simulated population mean $C_{ss,ave}$ of unbound ribociclib was 0.453, 2.608, 5.096 μmol/L, respectively, and the respective $K_{p,uu}$ was 1.84, 10.6, and 20.8. Notably, the predicted ribociclib tumor concentrations and extent of tumor penetration ($K_{p,uu}$) were accordance with the observed data in non-enhancing and enhancing tumor regions in glioblastoma

patients, showing the observed median (range) unbound ribociclib tumor concentrations of 0.458 (0.015–1.295) μmol/L and 1.644 (0.307–4.743) μmol/L respectively, and the observed $K_{p,uu}$ of 1.8 (0.7–11.3) and 10.1 (2.4–37.4) respectively.[12] Collectively, these data suggested that the developed 4Brain model well predicted the CNS pharmacokinetics of ribociclib as observed in glioblastoma patients. Therefore, the system-specific parameters for the 4Brain model (e.g., the transporter relative activity factors at the BBB and blood-CSF barrier) were verified, and could be confidently applied to predict the CNS pharmacokinetics of palbociclib and abemaciclib (for which no or limited clinical CNS data were available).

The model-simulated steady-state concentrations of unbound abemaciclib and palbociclib in the human normal brain and CSF are summarized in Table 3. For abemaciclib, limited CSF data were obtained from 10 patients following varying dosing regimens (i.e., daily or twice daily oral dosing at 50 – 275 mg for 15 days).[14] A direct comparison between the observed and predicted abemaciclib CSF data was not feasible because of varying dosing regimens and varying sampling times in the reported clinical study. Nevertheless, the observed abemaciclib CSF concentrations (range, 0.004 to 0.030 μmol/L) generally overlapped with the predicted data (population mean $C_{ss,ave}$, 0.038 μmol/L; 5^{th} and 95^{th} percentiles, 0.013 – 0.091 μmol/L) following the standard dosing regimen (150 mg BID for 28 days). In addition, the predicted mean CSF $K_{p,uu}$ was 1.10-fold of the observed data (predicted vs. observed mean, 0.77 vs. 0.70).

For palbociclib, no clinical CNS pharmacokinetic data was available. Preclinical studies showed that the brain penetration of palbociclib ($K_{p,uu}$, 0.01 in rats and mice) was approximately 10-fold less than that of abemaciclib ($K_{p,uu}$, 0.11 in rats and 0.17 in mice).[15] Despite the species difference in the absolute $K_{p,uu}$ values between humans and rodents, the model-predicted 10-fold less brain penetration of palbociclib than abemaciclib in humans ($K_{p,uu}$, 0.12 vs. 1.04) was consistent with preclinical observation. The brain penetration of ABCB1 substrates is expected to be larger in humans than rodents because ABCB1 protein abundance is significantly lower at the human BBB than rodent BBB and also because of species difference in the CSF dynamics and brain physiology.[20,26] For example, the brain penetration ($K_{p,uu}$) of ABCB1 substrate drugs (including verapamil, GR205171, altanserin, and AZD1775) has been reported to be several to over 10-fold greater in humans than in rodents.[19,27,28]

Comparison of the CNS pharmacokinetics between the three CDK4/6 inhibitors—Ribociclib and palbociclib are similar with respect to the chemical structure, physicochemical properties, binding to plasma proteins and brain tissues, as well as intrinsic passive transcellular permeability and intrinsic active efflux clearance; whereas, abemaciclib is significantly dissimilar than either one (Table 1 and 2). Therefore, it was not surprising that the CNS pharmacokinetics of abemaciclib was different from the other two CDK4/6 inhibitors, which was characterized by a slower brain penetration but to a larger extent (Figure 4A–4C). It is known that the rate of drug brain penetration is largely driven by the drug binding to brain tissue and passive or active efflux clearance at the BBB. Specifically, higher brain tissue binding and lower passive or active efflux clearance at the BBB lead to slower brain penetration.[19] Hence, the slower brain penetration of abemaciclib was expected

given its significantly higher brain tissue binding and lower passive and active efflux clearance at the BBB as compared to ribociclib and palbociclib.

Despite slow brain penetration, abemaciclib penetrated into the brain to a larger extent than the other two CDK4/6 inhibitors. The PBPK models predicted that ribociclib and palbociclib shared a similar brain $K_{p,uu}$ (~ 0.14 vs. 0.12), while abemaciclib had a $K_{p,uu}$ of ~ 1.0 (Table 3). It is known that the $K_{p,uu}$ (the extent of brain penetration) is determined by the relative contribution of passive clearance and transporter-mediated active clearance at the BBB.[29] If the BBB transport of a drug is dominated by passive permeability, the $K_{p,uu}$ would approach 1; whereas, when a drug is actively transported by efflux or uptake transporters at the BBB, the $K_{p,uu}$ would be smaller or larger than 1.0. While the three CDK4/6 inhibitors were ABCB1 substrates, abemaciclib showed approximately 30-fold lower ABCB1-mediated intrinsic efflux clearance as compared to ribociclib and palbociclib (Table 1). In addition, although palbociclib and abemaciclib were identified as the substrates for mouse abcg2,[15] our study suggested that palbociclib was a substrate of human ABCG2, but ribociclib and abemaciclib were not, at least not good, substrates for human ABCG2 (Table 2). ABCB1 and ABCG2 are two predominant efflux transporters at the human BBB, acting synergistically to restrict the brain penetration of dual ABCB1/ABCG2 substrates.[30–32] Palbociclib was a dual substrate for ABCB1 and ABCG2, while ribociclib and abemaciclib appeared to be transported mainly by ABCB1. Collectively, the IVIVE predicted that the overall efflux transporter-mediated *in vivo* efflux clearance at the human BBB was 1.0 L/h for abemaciclib, 22.8 L/h for ribociclib, and 40.3 L/h for palbociclib, which accounted for 0.2-, 6.4-, and 4.9-fold of their respective BBB passive clearance at a normal brain pH. These data suggested that the BBB transport of abemaciclib was dominated by passive permeability, while the BBB transport of ribociclib and palbociclib was dominated by active efflux.

Also noted was that the CSF pharmacokinetics of abemaciclib was different from the other two CDK4/6 inhibitors (Figure 4A, 4B, 4C). The predicted mean CSF-to-unbound plasma ratio of abemaciclib (CSF $K_{p,uu}$, 0.8) was close to its brain $K_{p,uu}$ (1.0), indicating that abemaciclib CSF concentration could be used as a surrogate for unbound brain concentration. By contrary, the predicted CSF $K_{p,uu}$ of ribociclib (~ 1.6) and palbociclib (~ 1.8) was > 10-fold of their respective brain $K_{p,uu}$, consistent with the predicted ~ 10-fold higher CSF concentrations than their respective unbound brain concentrations (Table 3). Drug penetration from the circulation blood to CSF is controlled by the blood-CSF barrier, which is formed by the choroid plexus epithelial cells and the arachnoid membrane.[33] ABCB1 expression has been identified on the apical, CSF-facing side of the blood-CSF barrier, suggesting that ABCB1 facilitates the transport of substrates into the CSF.[34,35] Therefore, the dominant ABCB1-mediated active CSF uptake of ribociclib and palbociclib at the blood-CSF barrier resulted in CSF $K_{p,uu}$ > 1.0. By contrary, ABCB1 played a minor role in the BBB or CSF penetration of abemaciclib because of the insignificant ABCB1 intrinsic clearance of abemaciclib. The PBPK model predictions supported the notion that CSF concentrations may be useful as a reflection of unbound drug brain concentrations for drugs (e.g., abemaciclib) that pass the BBB and blood-CSF barrier mainly by passive transcellular permeability, while for drugs (e.g., ribociclib and palbociclib) that undergo

dominant active transport at the BBB and blood-CSF barrier, the relationship between unbound drug brain and CSF concentrations may not be obvious.[36]

Refining dosing regimens—Target engagement ratio, defined as the ratio of the average steady-state unbound drug brain concentration to the *in vitro* IC_{50} for CDK4/6 inhibition, was used as a crude predictor of efficacy.[15] Theoretically, a target engagement ratio ≥ 1 would lead to 50% or greater inhibition of CDK4/6. Abemaciclib is the most potent CDK4/6 inhibitor (with the *in vitro* IC_{50} of 2 and 10 nM for inhibition of CDK4 and CDK6, respectively) as compared to palbociclib (IC_{50}, 11 and 15 nM) and ribociclib (IC_{50}, 10 and 39 nM).[13] Simulations following the standard dosing regimens suggested that the predicted population mean brain $C_{ss,ave}$ of unbound ribociclib, palbociclib, and abemaciclib were 0.024, 0.004, and 0.052 μmol/L, respectively, and correspondingly the CDK4/6 target engagement ratios were 2.4/0.62 for ribociclib, 0.36/0.27 for palbociclib, and 26/5.2 for abemaciclib (Table 3). Based on the criterion of target engagement ratio ≥ 1 required for potential clinical efficacy, abemaciclib achieved adequate inhibition for CDK4 and CDK6 in the human brain at the standard dosing regimen (150 mg BID). However, ribociclib may sufficiently inhibit CDK4, but not CDK6 in the brain at the standard dosing regimen (600 mg QD). Palbociclib did not achieve adequate brain concentrations to inhibit CDK4 or CDK6 following the standard dosing regimen (125 mg QD).

Additional simulations were performed to refine dosing regimens (Figure 4). Following 21-day treatment of ribociclib at the maximum tolerated dose (900 mg QD), the simulated population mean brain $C_{ss,ave}$ of unbound ribociclib was 0.036 μmol/L and the corresponding CDK4/6 target engagement ratios were 3.6/0.92 (Table 3), indicating that the treatment of ribociclib at the maximum tolerated dose may sufficiently inhibit both CDK4 and CDK6. However, palbociclib did not achieve sufficient brain concentration for CDK4/6 inhibition (target engagement ratios < 0.5) even at a dose 50% higher than the standard dose (Table 3). For abemaciclib, simulations suggested that 150 mg BID and 300 mg QD dosing resulted in comparable unbound brain exposure in terms of the maximum, trough, or average steady-state brain concentrations of unbound abemaciclib (Table 3).

DISCUSSION

Despite extensive efforts, progress in developing effective therapies for primary and metastatic brain cancer has been disappointing. Lack of efficacy may stem from genetically heterogeneous feature the tumor, emergence of intrinsic resistance mechanisms, and particularly, poor penetration of potentially effective therapeutic agents across the human BBB.[37–39] The BBB is a dynamic interface separating the brain parenchyma from the circulatory system, which protects the CNS from potentially harmful chemicals while regulating transport of essential molecules and maintaining the homeostasis of the CNS.[39] The structure and function of the BBB in brain tumors is often disrupted and heterogeneous.[40–42] For example, glioblastoma consists of different regions presenting various degrees of BBB integrity varying from completely compromised in bulky tumor areas, slightly “leaky” in invasive peripheral regions, and to completely intact in infiltrating tumor regions.[17,20,40–42] In spite of enhanced drug penetration into bulky tumor areas, insufficient penetration of potentially effective therapeutic agents into invasive, infiltrative tumor regions

or micro-metastases behind an intact BBB, which are often unresectable and give rise to recurrent disease, is a significant barrier to long-term, efficacious treatments.[17] Therefore, both primary and metastatic brain cancer should be treated as a disease of the whole brain. A potentially clinical successful therapeutic agent must penetrate across the intact human BBB to achieve adequate pharmacologically active concentrations in the brain. When selecting drug candidates and designing dosing regimens for brain cancer treatment, one needs consider the drug brain penetration, system pharmacokinetics, and potency for target inhibition.

The $K_{p,uu}$, as the measure of the extent of drug brain penetration, is a key parameter considered in CNS drug discovery and development. Nevertheless, it should be emphasized that brain exposure to unbound drug, which drives pharmacological activity and efficacy, is determined by both the $K_{p,uu}$ and systemic (or plasma) drug exposure. PBPK model simulations, supported by *in vitro* cellular permeability and transporter kinetic data, suggest that the transport of abemaciclib at the human BBB is dominated by passive permeability resulting in a $K_{p,uu}$ approximately 1.0, while the transport of ribociclib ($K_{p,uu}$ 0.14) and palbociclib ($K_{p,uu}$ 0.12) is dominated by ABCB1/ABCG2-mediated active efflux. Notably, while ribociclib and palbociclib share similar $K_{p,uu}$, unbound ribociclib brain concentration is > 5-fold higher than palbociclib following the standard dosing regimens (Table 3). Likewise, although the extent of brain penetration of abemaciclib is ~ 7-fold larger than ribociclib ($K_{p,uu}$, 1.0 vs. 0.14), the brain exposure to two drugs only differs by about 2-fold following the standard dosing regimens (Table 3). The relatively higher unbound ribociclib brain exposure is largely driven by its higher unbound plasma exposure. For example, the population mean plasma $C_{ss,ave}$ of unbound ribociclib is ~ 6.0- and 3.5-fold of that for palbociclib and abemaciclib, respectively, following the standard dosing regimens (Table 3). Hence, in spite of a relatively low $K_{p,uu}$, ribociclib has the potential to achieve adequate target inhibition in the brain at the maximum tolerate dose. These data underscore the importance for consideration of not only the extend of brain penetration ($K_{p,uu}$) but also drug plasma exposure achievable at a safe or tolerable when selecting candidate drugs for brain cancer treatment.

Another critical consideration is the drug potency for target inhibition. In light of the notion that adequate target inhibition is the prerequisite for clinical efficacy, the target engagement ratio, which takes into account both unbound drug brain concentration and the potency for target inhibition, appears to be the best criteria for selection of brain cancer therapeutic agents. It has been demonstrated that the adequate inhibition of cyclin D-CDK4/6-Rb pathway (as indicated by a decrease in pRb more than 60% in skin) is significantly associated with the clinical efficacy (stable disease or response) of abemaciclib in patients with HR-positive breast cancer.[14] In our study, a target engagement ratio ≥ 1 achieved in the normal brain is used as the threshold to ensure CDK4/6 inhibition in brain tumors especially in microscopic tumor regions behind an intact BBB. Abemaciclib is the most potent CDK4/6 inhibitor as compared to palbociclib and ribociclib.[13] In addition, abemaciclib exhibits excellent brain penetration ($K_{p,uu}$, 1.0) and reasonably good systemic exposure. These together lead to abemaciclib target engagement ratio of 26 (for CDK4) and 5.2 (for CDK6) following the standard dosing regimen. The potential clinical efficacy of abemaciclib for brain cancer treatment has been demonstrated in a phase I/II clinical trial where 3

glioblastoma patients achieved stable disease on single-agent abemaciclib treatment, and 2 of them continued the treatment without progression for nearly 2 years.[14] By contrary, because of the low brain exposure and modest potency of palbociclib, the CDK4/6 target engagement ratio is < 0.5 even at a dose 50% higher than the standard dose. On the other hand, due to the relatively low potency for CDK4/6 inhibition, ribociclib may sufficiently inhibit CDK4 (target engagement ratio, 2.4) but not CDK6 (target engagement ratio, 0.62) although it achieves similar brain exposure as abemaciclib following the standard dosing regimens. These data collectively suggest that abemaciclib is the best CDK4/6 inhibitor for brain cancer treatment, while palbociclib is not recommended to use. Ribociclib has the potential to sufficiently inhibit both CDK4 and CDK6 at the maximum tolerated dose.

Different dosing strategies have been used for the three CDK4/6 inhibitors in the treatment of breast cancer, given their different system pharmacokinetics and clinical toxicities. Due to significant myelotoxicity, ribociclib and palbociclib require an intermittent dosing schedule (3-weeks-on/1-week-off) to allow bone marrow recovery. By contrast, abemaciclib has a safety profile allowing continuous dosing schedule (4-week-on), which provides important opportunities for combining abemaciclib with a variety of targeted or cytotoxic agents. Previous clinical study suggests that the administration of abemaciclib at 200 mg or 150 mg BID can achieve sustained pharmacodynamic effects in proliferating kerotinocytes and tumors in patients with non-CNS cancers including breast cancer, non-small cell lung cancer, and melanoma.[14] Hence, 200 mg and 150 mg BID was recommended as the starting dose for single-agent and combination treatment, respectively. However, because of the reasonable plasma elimination half-life of abemaciclib (observed vs. PBPK-model predicted population mean $T_{1/2}$, 22 vs. 20 h) and a broad dose range associated with clinical efficacy, once daily dosing schedule may also achieve sustained target inhibition in the human brain. PBPK simulations suggest that 150 mg BID and 300 mg QD dosing result in comparable plasma or brain exposure to unbound abemaciclib in terms of the maximum, trough, or average steady-state concentrations (Table 3 and Figure 4). Notably, similar to slow-released formulations, the slow BBB penetration and sustained brain retention of abemaciclib result in a small fluctuation between the peak and trough steady-state brain concentrations following either twice daily or once daily dosing (Figure 4). Thus, 300 mg QD dosing would be expected to produce a similar, if not better, safety profile and clinical efficacy as 150 mg BID dosing. Considering the treatment convenience and likely better safety profile for once daily dosing, it would be reasonable to initiate abemaciclib for brain cancer treatment at 300 mg QD on a 4-weeks-on continuous schedule. Further prospective clinical trials are needed to confirm the refined dosing regimen.

Supplementary Material

Refer to Web version on PubMed Central for supplementary material.

Acknowledgments

Funding: The United States National Institute of Health (NIH) Cancer Center Support Grant P30 CA022453.

REFERENCES

1. Batich KA & Sampson JH Standard of care and future pharmacological treatment options for malignant glioma: an urgent need for screening and identification of novel tumor-specific antigens. Expert Opin Pharmacother 15, 2047–61 (2014). [PubMed: 25139628]
2. Ohgaki H & Kleihues P Epidemiology and etiology of gliomas. Acta Neuropathol 109, 93–108 (2005). [PubMed: 15685439]
3. Gavrilovic IT & Posner JB Brain metastases: epidemiology and pathophysiology. Journal of neuro-oncology 75, 5–14 (2005). [PubMed: 16215811]
4. Sperduto PW et al. Summary report on the graded prognostic assessment: an accurate and facile diagnosis-specific tool to estimate survival for patients with brain metastases. Journal of clinical oncology : official journal of the American Society of Clinical Oncology 30, 419–25 (2012). [PubMed: 22203767]
5. Hall M & Peters G Genetic alterations of cyclins, cyclin-dependent kinases, and Cdk inhibitors in human cancer. Adv Cancer Res 68, 67–108 (1996). [PubMed: 8712071]
6. Sherr CJ Cancer cell cycles. Science 274, 1672–7 (1996). [PubMed: 8939849]
7. Shapiro GI Cyclin-dependent kinase pathways as targets for cancer treatment. J Clin Oncol 24, 1770–83 (2006). [PubMed: 16603719]
8. Yu Q et al. Requirement for CDK4 kinase function in breast cancer. Cancer Cell 9, 23–32 (2006). [PubMed: 16413469]
9. Choi YJ et al. The requirement for cyclin D function in tumor maintenance. Cancer Cell 22, 438–51 (2012). [PubMed: 23079655]
10. Shah M, Nunes MR & Stearns V CDK4/6 Inhibitors: Game Changers in the Management of Hormone Receptor-Positive Advanced Breast Cancer? Oncology (Williston Park) 32, 216–22 (2018). [PubMed: 29847850]
11. Geoerger B et al. A Phase I Study of the CDK4/6 Inhibitor Ribociclib (LEE011) in Pediatric Patients with Malignant Rhabdoid Tumors, Neuroblastoma, and Other Solid Tumors. Clin Cancer Res 23, 2433–41 (2017). [PubMed: 28432176]
12. Tien AC et al. A Phase 0 Trial of Ribociclib in Recurrent Glioblastoma Patients Incorporating a Tumor Pharmacodynamic- and Pharmacokinetic-Guided Expansion Cohort. Clin Cancer Res 25, 5777–86 (2019). [PubMed: 31285369]
13. Klein ME, Kovatcheva M, Davis LE, Tap WD & Koff A CDK4/6 Inhibitors: The Mechanism of Action May Not Be as Simple as Once Thought. Cancer Cell 34, 9–20 (2018). [PubMed: 29731395]
14. Patnaik A et al. Efficacy and Safety of Abemaciclib, an Inhibitor of CDK4 and CDK6, for Patients with Breast Cancer, Non-Small Cell Lung Cancer, and Other Solid Tumors. Cancer Discov 6, 740–53 (2016). [PubMed: 27217383]
15. Raub TJ et al. Brain Exposure of Two Selective Dual CDK4 and CDK6 Inhibitors and the Antitumor Activity of CDK4 and CDK6 Inhibition in Combination with Temozolomide in an Intracranial Glioblastoma Xenograft. Drug Metab Dispos 43, 1360–71 (2015). [PubMed: 26149830]
16. Parrish KE, Pokorny J, Mittapalli RK, Bakken K, Sarkaria JN & Elmquist WF Efflux transporters at the blood-brain barrier limit delivery and efficacy of cyclin-dependent kinase 4/6 inhibitor palbociclib (PD-0332991) in an orthotopic brain tumor model. J Pharmacol Exp Ther 355, 264–71 (2015). [PubMed: 26354993]
17. Sarkaria JN et al. Is the blood-brain barrier really disrupted in all glioblastomas? A critical assessment of existing clinical data. Neuro Oncol 20, 184–91 (2018). [PubMed: 29016900]
18. Jones H & Rowland-Yeo K Basic concepts in physiologically based pharmacokinetic modeling in drug discovery and development. CPT Pharmacometrics Syst Pharmacol 2, e63 (2013). [PubMed: 23945604]
19. Li J et al. Quantitative and Mechanistic Understanding of AZD1775 Penetration across Human Blood-Brain Barrier in Glioblastoma Patients Using an IVIVE-PBPK Modeling Approach. Clin Cancer Res 23, 7454–66 (2017). [PubMed: 28928160]

20. Bao X et al. Protein Expression and Functional Relevance of Efflux and Uptake Drug Transporters at the Blood-Brain Barrier of Human Brain and Glioblastoma. Clin Pharmacol Ther, (2019).
21. Tate SC, Sykes AK, Kulanthaivel P, Chan EM, Turner PK & Cronier DM A Population Pharmacokinetic and Pharmacodynamic Analysis of Abemaciclib in a Phase I Clinical Trial in Cancer Patients. Clin Pharmacokinet 57, 335–44 (2018). [PubMed: 28540640]
22. De Luca A et al. Pharmacokinetic drug evaluation of palbociclib for the treatment of breast cancer. Expert Opin Drug Metab Toxicol 14, 891–900 (2018). [PubMed: 30130984]
23. Honasoge A & Sontheimer H Involvement of tumor acidification in brain cancer pathophysiology. Front Physiol 4, 316 (2013). [PubMed: 24198789]
24. Zhang X, Lin Y & Gillies RJ Tumor pH and its measurement. J Nucl Med 51, 1167–70 (2010). [PubMed: 20660380]
25. Casey JR, Grinstein S & Orlowski J Sensors and regulators of intracellular pH. Nat Rev Mol Cell Biol 11, 50–61 (2010). [PubMed: 19997129]
26. de Lange EC Utility of CSF in translational neuroscience. J Pharmacokinet Pharmacodyn 40, 315–26 (2013). [PubMed: 23400635]
27. Syvanen S et al. Species differences in blood-brain barrier transport of three positron emission tomography radioligands with emphasis on P-glycoprotein transport. Drug metabolism and disposition: the biological fate of chemicals 37, 635–43 (2009). [PubMed: 19047468]
28. Pokorny JL et al. The Efficacy of the Wee1 Inhibitor MK-1775 Combined with Temozolomide Is Limited by Heterogeneous Distribution across the Blood-Brain Barrier in Glioblastoma. Clinical cancer research : an official journal of the American Association for Cancer Research 21, 1916–24 (2015). [PubMed: 25609063]
29. Hammarlund-Udenaes M, Friden M, Syvanen S & Gupta A On the rate and extent of drug delivery to the brain. Pharmaceutical research 25, 1737–50 (2008). [PubMed: 18058202]
30. Bauer M et al. Pilot PET Study to Assess the Functional Interplay Between ABCB1 and ABCG2 at the Human Blood-Brain Barrier. Clinical pharmacology and therapeutics 100, 131–41 (2016). [PubMed: 26940368]
31. Polli JW et al. An unexpected synergist role of P-glycoprotein and breast cancer resistance protein on the central nervous system penetration of the tyrosine kinase inhibitor lapatinib (N-{3-chloro-4-[(3-fluorobenzyl)oxy]phenyl}−6-[5-({[2-(methylsulfonyl)ethyl]amino }methyl)-2-furyl]-4-quinazolinamine; GW572016). Drug metabolism and disposition: the biological fate of chemicals 37, 439–42 (2009). [PubMed: 19056914]
32. Zamek-Gliszczynski MJ, Kalvass JC, Pollack GM & Brouwer KL Relationship between drug/metabolite exposure and impairment of excretory transport function. Drug metabolism and disposition: the biological fate of chemicals 37, 386–90 (2009). [PubMed: 19022942]
33. Redzic Z Molecular biology of the blood-brain and the blood-cerebrospinal fluid barriers: similarities and differences. Fluids Barriers CNS 8, 3 (2011). [PubMed: 21349151]
34. Daood M, Tsai C, Ahdab-Barmada M & Watchko JF ABC transporter (P-gp/ABCB1, MRP1/ABCC1, BCRP/ABCG2) expression in the developing human CNS. Neuropediatrics 39, 211–8 (2008). [PubMed: 19165709]
35. Rao VV et al. Choroid plexus epithelial expression of MDR1 P glycoprotein and multidrug resistance-associated protein contribute to the blood-cerebrospinal-fluid drug-permeability barrier. Proc Natl Acad Sci U S A 96, 3900–5 (1999). [PubMed: 10097135]
36. de Lange EC & Danhof M Considerations in the use of cerebrospinal fluid pharmacokinetics to predict brain target concentrations in the clinical setting: implications of the barriers between blood and brain. Clin Pharmacokinet 41, 691–703 (2002). [PubMed: 12162757]
37. Miller JJ & Wen PY Emerging targeted therapies for glioma. Expert Opin Emerg Drugs 21, 441–52 (2016). [PubMed: 27809598]
38. Henderson JT & Piquette-Miller M Blood-brain barrier: an impediment to neuropharmaceuticals. Clin Pharmacol Ther 97, 308–13 (2015). [PubMed: 25670372]
39. Bhowmik A, Khan R & Ghosh MK Blood brain barrier: a challenge for effectual therapy of brain tumors. Biomed Res Int 2015, 320941 (2015). [PubMed: 25866775]

40. Watkins S, Robel S, Kimbrough IF, Robert SM, Ellis-Davies G & Sontheimer H Disruption of astrocyte-vascular coupling and the blood-brain barrier by invading glioma cells. Nat Commun 5, 4196 (2014). [PubMed: 24943270]

41. Lockman PR et al. Heterogeneous blood-tumor barrier permeability determines drug efficacy in experimental brain metastases of breast cancer. Clin Cancer Res 16, 5664–78 (2010). [PubMed: 20829328]

42. Gerstner ER & Fine RL Increased permeability of the blood-brain barrier to chemotherapy in metastatic brain tumors: establishing a treatment paradigm. Journal of clinical oncology : official journal of the American Society of Clinical Oncology 25, 2306–12 (2007). [PubMed: 17538177]

Study Highlights

What is the current knowledge on the topic?

CDK4/6 inhibitors (ribociclib, palbociclib, and abemaciclib) are under clinical development for treating primary and metastatic brain cancer. Sufficient drug penetration across the human blood-brain barrier (BBB) is the prerequisite for sustained *in vivo* target inhibition and efficacious treatment of brain cancer. Selection of the drug with favorable central nervous system (CNS) pharmacokinetics and design of optimal dosing regimen will maximize the success of the development and treatment. However, the human CNS pharmacokinetics of the CDK4/6 inhibitors remain understudied and poorly understood.

What question did this study address?

Using the PBPK modeling approach, we systematically compared the human CNS pharmacokinetics of the three CDK4/6 inhibitors.

What does this study add to our knowledge?

The PBPK modeling, supported by available preclinical and clinical evidence, suggests that abemaciclib is the best CDK4/6 inhibitor for brain cancer treatment, while palbociclib is not recommended. The model refined dosing regimen is 300 mg daily on a 4-weeks-on schedule for abemaciclib, and 900 mg daily on a 3-weeks-on/1-week-off schedule for ribociclib. Further prospective clinical trials are needed to confirm this.

How might this change clinical pharmacology or translational science?

Our study composes a framework for the application of mechanism-based PBPK modeling to guide selection of the right drug and refinement of dosing regimen for more effective treatment of brain cancer.

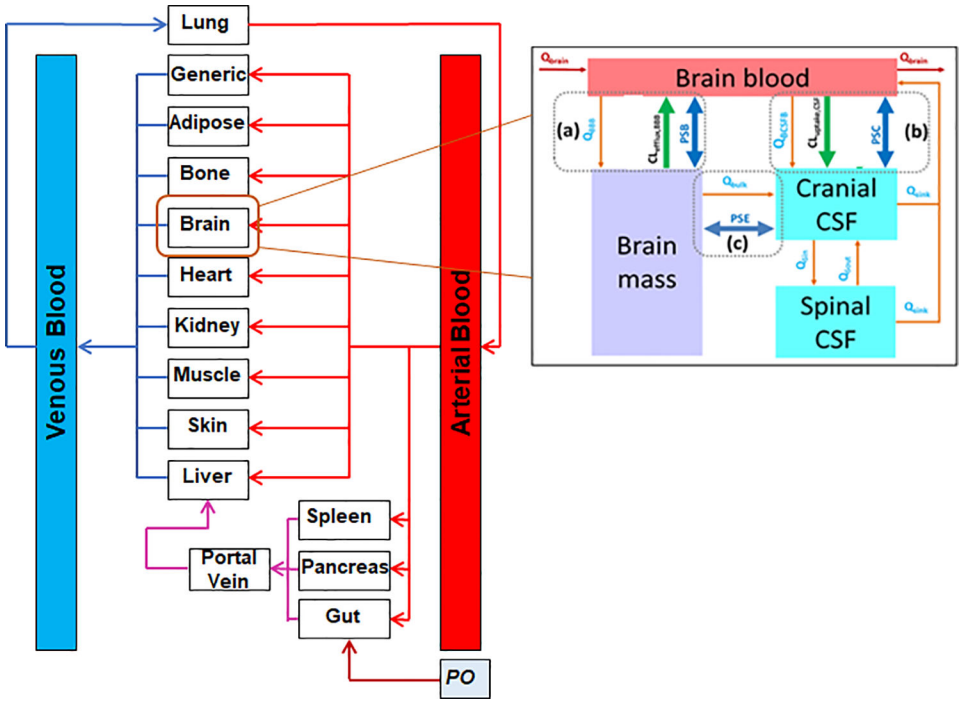

Figure 1.

Model structure of the whole-body PBPK model integrated with a 4-compartment permeability-limited brain (4Brain) model, which has 4 compartments representing the brain blood, brain mass, cranial cerebrospinal fluid (CSF), and spinal CSF. The 4Brain model assumes: 1) drug transport across the BBB is governed by bi-directional passive permeability (PSB) and ABCB1- and ABCG2-mediated active efflux clearance ($CL_{efflux,BBB}$); 2) drug transport across the blood-CSF barrier was controlled by bidirectional passive permeability (PSC) and ABCB1-mediated active influx clearance ($CL_{uptake,CSF}$); 3) drug transport between the brain mass and cranial CSF is diffusive transport at a bi-directional clearance (PSE); 4) fluid balance is maintained by the circulation of CSF between spinal and cranial compartments and reabsorbed into the brain blood; 5) the cerebral blood flow rate (Q_{Brain}) links the 4Bain model to whole-body model; 6) only unbound and unionized drug can passively pass through all barriers, while transporters act upon unbound drug (including both unionized and ionized species); 7) metabolism in brain mass is negligible; and 8) all compartments are well-stirred with defined volumes. Flow rates are described by the CSF secretion rate ($Q_{BCSFB)}$, bulk flow rate from brain mass to cranial CSF (Q_{bulk}), CSF flow rate out of cranial and spinal compartments (Q_{sink}), CSF shuttle flow rate between cranial and spinal compartments (Q_{Sin} and Q_{Sout}), and water transfer rate from the brain blood to brain mass (Q_{BBB}).

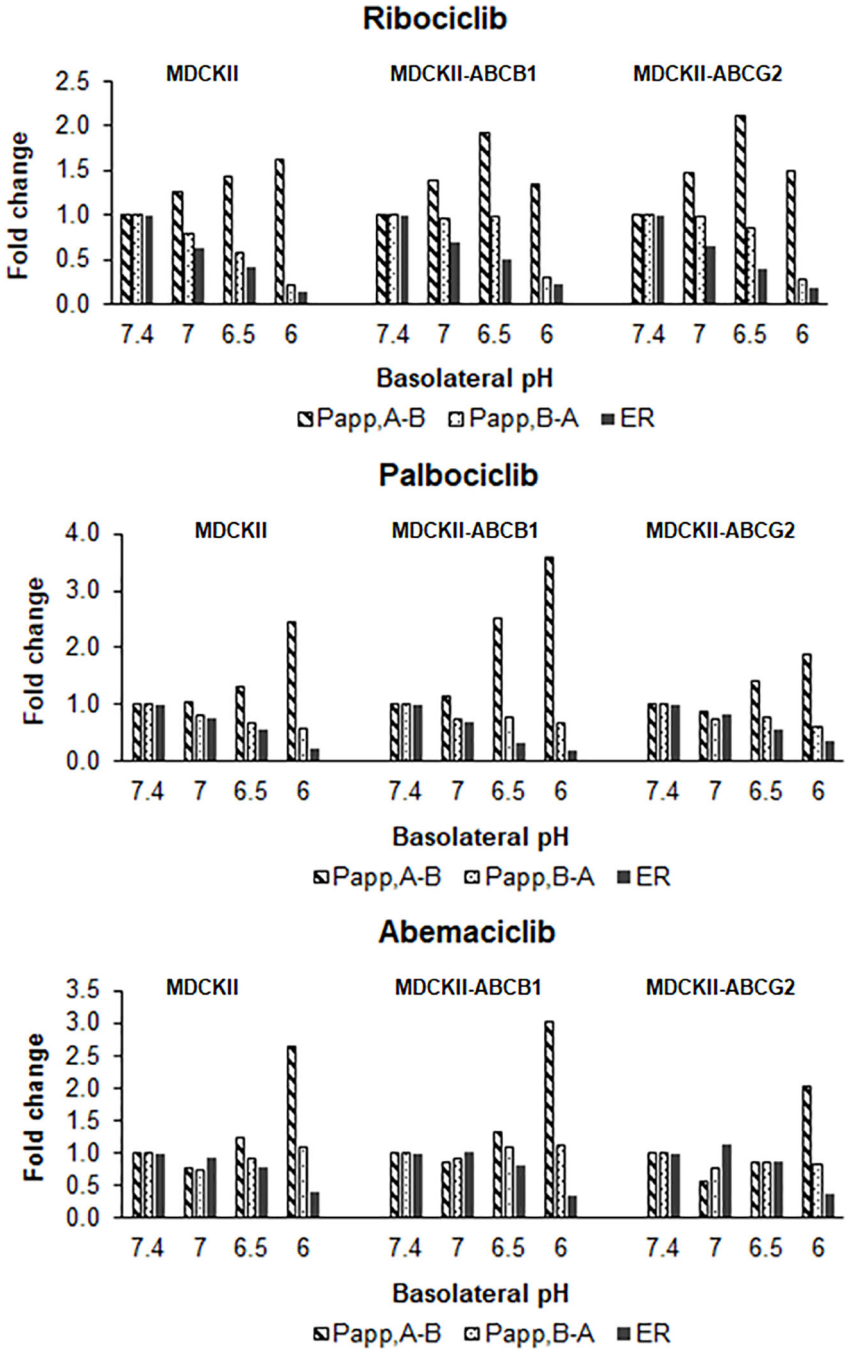

Figure 2.

pH-dependent apparent permeability of the three CDK4/6 inhibitors across the MDCKII, MDCKII-ABCB1, and MDCKII-ABCG2 cell monolayers. Bi-directional permeability experiments were performed at a fixed apical pH (7.4) and varying basolateral pH (7.4, 7.0, 6.5, and 6.0). The apparent permeability in the apical-to-basolateral ($P_{app,A-B}$) and basolateral-to-apical ($P_{app,B-A}$) directions and efflux ratio (ER) are expressed as the mean fold change relative to those determined in the control (at pH 7.4 in both apical and basolateral chambers).

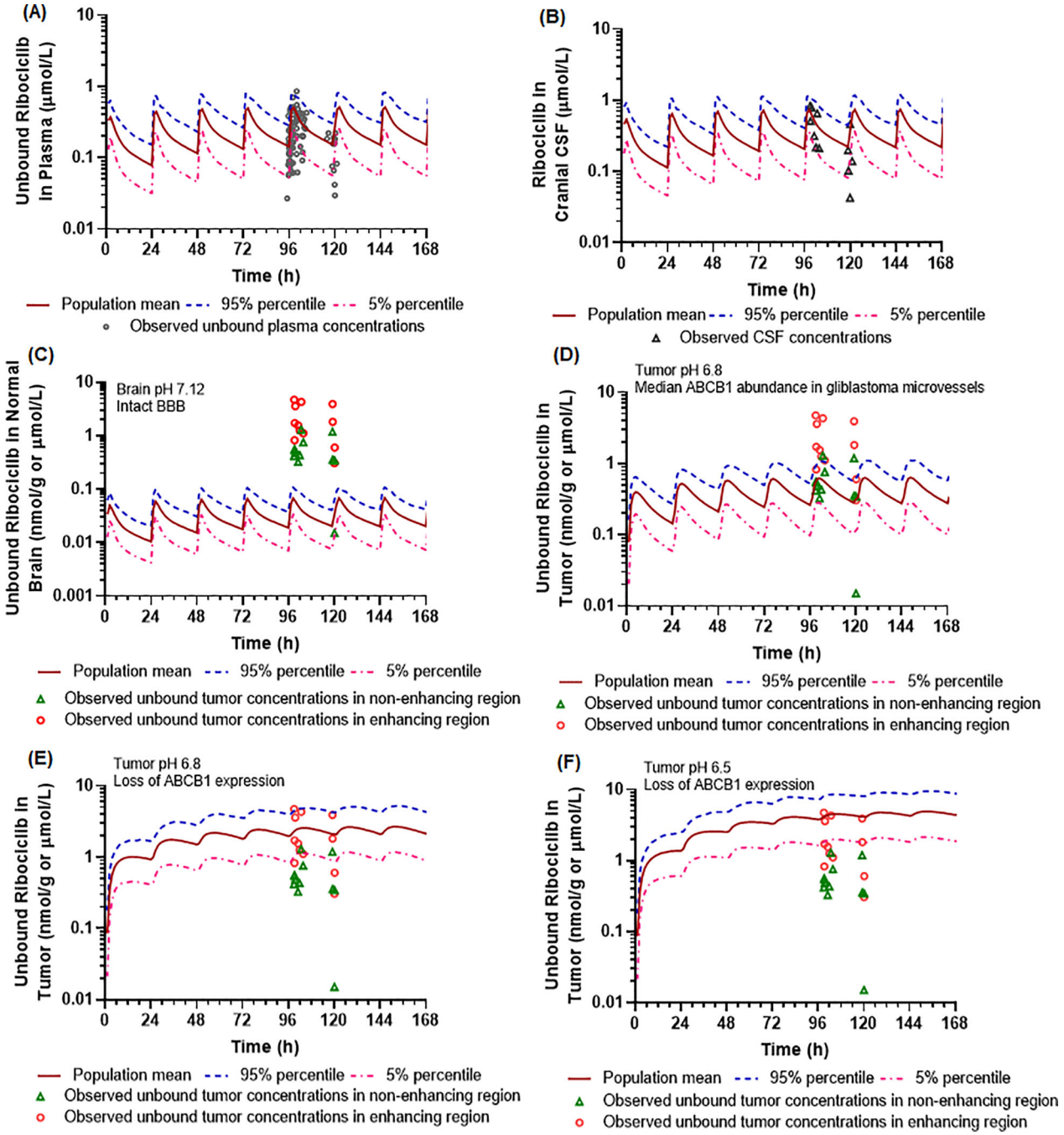

Figure 3.

PBPK model-simulated and clinically observed plasma and CNS pharmacokinetics of ribociclib. **(A)** Simulated and observed unbound ribociclib plasma concentration-time profiles. **(B)** Simulated and observed ribociclib CSF concentration-time profiles. **(C)** Simulated unbound ribociclib brain concentration-time profiles in the human normal brain (with brain pH 7.12 and ABCB1 abundance 3.38 pmol/mg at the BBB). **(D)** Simulated unbound ribociclib concentration-time profiles in brain tumors with pH 6.8 and ABCB1 abundance 0.14 pmol/mg at the BBB. **(E)** Simulated unbound ribociclib concentration-time

profiles in brain tumors with pH 6.8 and loss of ABCB1 expression at the BBB. **(F)** Simulated unbound ribociclib concentration-time profiles in brain tumors with pH 6.5 and loss of ABCB1 expression at the BBB. Simulations of 10 trials with 10 subjects in each were performed in the Simcyp virtual cancer patient population following 5-day ribociclib treatment at a daily oral dose of 900 mg. Observed clinical plasma and CNS pharmacokinetic data were obtained from 12 glioblastoma patients treated with ribociclib (900 mg QD for 5 days).

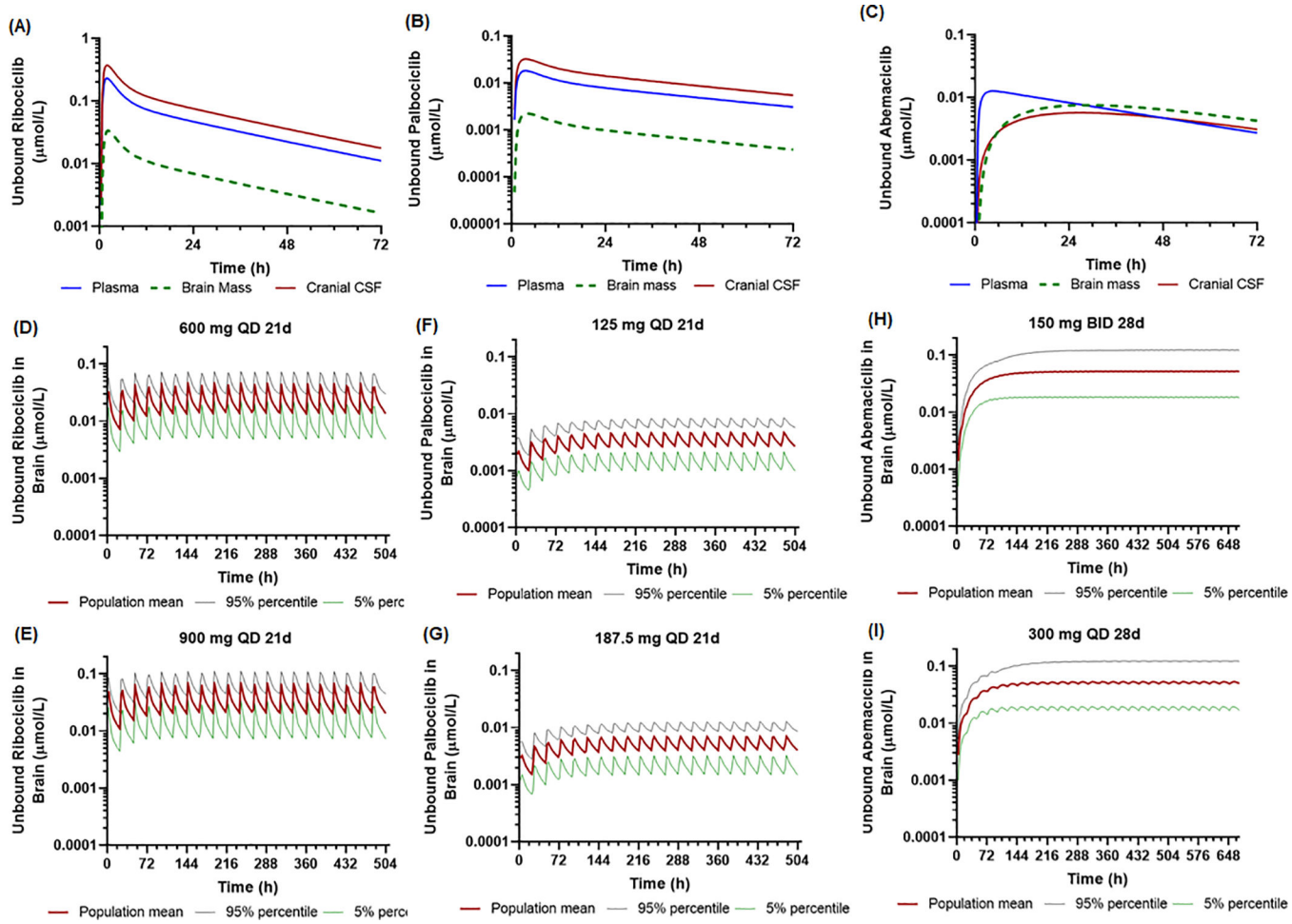

Figure 4.

PBPK model-simulated plasma and CNS pharmacokinetics of the three CDK4/6 inhibitors following varying dosing regimens. **(A)** Simulated population mean plasma, CSF, and brain concentration time profiles of unbound ribociclib following a single oral dose (600 mg). **(B)** Simulated population mean plasma, CSF, and brain concentration time profiles of unbound palbociclib following a single oral dose (125 mg). **(C)** Simulated population mean plasma, CSF, and brain concentration time profiles of unbound abemaciclib following a single oral dose (150 mg). **(D and E)** Simulated unbound ribociclib brain concentration time profiles following the standard dosing regimen (600 mg QD for 3-weeks) and modified dosing regimen (900 mg QD for 3 weeks). **(F and G)** Simulated unbound palbociclib brain concentration time profiles following the standard dosing regimen (125 mg QD for 3-weeks) and modified dosing regimen (187 mg QD for 3 weeks). **(H and I)** Simulated unbound abemaciclib brain concentration time profiles following the standard dosing regimen (150 mg BID for 4-weeks) and modified dosing regimen (300 mg QD for 4 weeks). Simulations of 10 trials with 10 subjects in each trial were performed in the Simcyp virtual cancer patient population.

Table 1

Drug-specific parameters in the whole-body-4Brain PBPK models

	Ribociclib	Palbociclib	Abemaciclib	Comments/Reference
Physicochemical				
MW (g/mol)	434.6	447.5	506.6	PubChem
LogP	2.38	2.77	4.25	ChemAxon
PKa1 (strongest acidic)	11.59	11.34	10.27	ChemAxon
PKa2 (strongest basic)	8.87	8.86	7.94	ChemAxon
B/P	1.5	1.9	1.2	Investigator brochure
$f_{u,p}$	0.125	0.126	0.06	Experimental determined
Absorption				
Fa	0.9	0.5	0.6	Assigned
Ka	0.8	0.367	0.197	Observed
Lag time (h)	0.5	0.658	0.5	Observed
fu_{gut}	0.0061	0.007	0.004	Simcyp predicted
Q_{gut} (L/h)	9.61	14.48	11.08	Simcyp predicted
Distribution				
V_{ss} (L/kg)	12.19	16.31	7.86	Predicted by Method 3, K_p scalar of 1
Elimination				
Human liver microsomes (HLM):				
V_{max} (pmol/min/mg)	313.7	518.5	2003	Experimental determined from HLM
K_m (μM)	13.4	78.1	126.2	Experimental determined from HLM
CL_{int} (μL/min/mg)	23.4	6.64	15.9	Experimental determined from HLM
fu_{inc}	0.35	0.2	0.2	Experimental determined from HLM
Human intestinal microsomes (HIM):				
V_{max} (pmol/min/mg)	104.8	280.7	494.3	Experimental determined from HIM
K_m (μM)	28.8	70.4	115.1	Experimental determined from HIM
CL_{int} (μL/min/mg)	3.64	3.99	4.29	Experimental determined from HIM
fu_{mic}	0.35	0.2	0.2	Experimental determined
CL_R (L/h)	7.5	10.5	1.5	Assigned
4Brain model				
Blood-brain barrier				
PSB (L/h)	135	307	25	Estimated by Eq. 1[a]
$f_{u,br}$	0.044	0.015	0.006	Experimental determined from patient brain tumor tissue
$CL_{ABCB1,vitro}$ (μL/min/mg)	21770	26160	800	Experimental determined Eq. 2[b]
$CL_{ABCG2,vitro}$ (μL/min/mg)	0	8580	90	Experimental determined Eq. 2[b]
ABCB1 RAF at BBB	87.3	87.3	87.3	Determined based on ABCB1 abundance in normal human brain microvessels by Eq.3[c]

	Ribociclib	Palbociclib	Abemaciclib	Comments/Reference
ABCB1 RAF at BBTB	5.88	5.88	5.88	Determined based on ABCB1 abundance in human glioblastoma microvessels by Eq.3[c]
ABCG2 RAF at BBB	125.3	125.3	125.3	Determined based on ABCG2 abundance in normal human brain microvessels by Eq.3[c]
ABCG2 RAF at BBTB	55.47	55.47	55.47	Determined based on ABCG2 abundance in human glioblastoma microvessels by Eq.3[c]
Blood-CSF barrier				
PSC (L/h)	67.5	150	13	Assumed to be half of PSB
fu_{csf}	1	1	1	Assigned given low CSF protein concentration
$CL_{ABCB1,vitro}$ (μL/min/mg)	21770	26160	800	Experimental determined Eq. 2[b]
ABCB1 RAF at BCCSF	8.7	8.7	8.7	Assigned and validated by observed ribociclib CSF data
Brain-cranial CSF barrier				
PSE (L/h)	300	300	300	Assigned assuming no barrier function

[a] $PSB = \frac{P_{app,\,A-B} \times SA}{\lambda}$ (Eq. 1), where $P_{app,A\rightarrow B}$ is the apparent permeability determined from MDCKII cell monolayer; SA is the human brain microvasculature surface area (mean, 20 m^2); and λ is unionization efficiency.

[b] $CL_{efflux,\,vitro} = \frac{2 \times P_{app,\,A-B} \times (NER - 1) \times SA}{\lambda \times Pro_{cell}}$ (Eq. 2), where $CL_{efflux,vitro}$ (μL/min/mg) is the *in vitro* efflux transporter-mediated intrinsic clearance; NER is the net efflux ratio determined from MDCKII-ABCB1or MDCKII–ABCG2; $P_{app,A-B}$ is the apparent passive permeability determined from MDCKII; SA is the filter surface area (0.143 cm^2) in a 96-well transwell; λ is unionization efficiency; and Pro_{cell} is the cell membrane protein amount in a 96-well transwell.

[c] $RAF = \frac{Abundance\ in\ vivo}{Abundance\ in\ vitro} \times BMvPGB \times BW$ (Eq. 3), where RAF is the relative activity factor; BMvPGB is the milligrams of brain microvessels per gram brain; BW is the average human brain weight; abundance *in vivo* or *in vitro* represents the ABCB1/ABCG2 transporter protein expression level in human brain microvessels or in MDCKII-ABCB1 and –ABCG2 cells, respectively.

Abbreviations: B/P, blood-to-plasma partition ratio; $CL_{ABCB1,vitro}$ and $CL_{ABCB1,vitro}$, ABCB1- and ABCG2-mediated in vitro efflux clearance, respectively; CL_{int}, *in vitro* intrinsic metabolic clearance; CL_R, renal clearance; $f_{u,br}$, fraction unbound drug in brain tissue; $f_{u,p}$, fraction of unbound drug in plasma; fu_{csf}, fraction unbound in CSF; fu_{gut}, fraction of unbound drug in enterocytes; fu_{mic}, fraction of unbound in microsomal incubation; K_m, substrate concentration at which half of V_{max} is achieved; logP, logarithm of the neutral species octanol-to-buffer partition ratio; MW, molecule weight; PK_a, acid dissociation constant; PSB, passive permeability-surface area product at the BBB; PSC, passive permeability-surface area product at the blood-cranial CSF barrier; PSE, passive permeability-surface area product at the brain-cranial CSF barrier; Q_{gut}, gut blood flow; RAF, in vivo-in vitro relative activity factor; V_{max}, maximum metabolic rate; V_{ss}, volume of distribution at steady-state.

Table 2

Transcellular permeability and efflux ratios of the three CDK4/6 inhibitors, determined from the parental MDCKII, MDCKII-ABCB1, and MDCKII-ABCG2 cell monolayers

	Ribociclib	Palbociclib	Abemaciclib
Parental MDCKII			
Apparent permeability ($P_{app,A-B}$) ($\times 10^{-6}$ cm/s)[a]	7.17 ± 1.85	9.38 ± 1.16	9.09 ± 2.21
Net efflux ratio[b]	1.02 ± 0.21	1.55 ± 0.17	1.03 ± 0.30
Unionization efficiency (λ)[c]	0.033	0.034	0.224
Intrinsic permeability ($P_{app,A-B}$/ λ)[d]	218.6	280.0	40.6
MDCKII-ABCB1			
Apparent permeability ($P_{app,A-B}$) ($\times 10^{-6}$ cm/s)[a]	1.77 ± 0.82	5.56 ± 1.10	5.65 ± 0.86
Net efflux ratio[b]	10.5 ± 3.30	5.92 ± 1.04	2.84 ± 0.49
MDCKII-ABCG2			
Apparent permeability $P_{app,A-B}$ ($\times 10^{-6}$ cm/s)[a]	5.90 ± 0.91	7.73 ± 0.25	7.98 ± 0.42
Net efflux ratio[b]	1.02 ± 0.20	2.64 ± 1.05	1.21 ± 0.11

[a] Bidirectional permeability experiments were performed at pH 7.4 in both apical and basolateral chambers.

[b] Net efflux ratio was the efflux ratio in the absence of an ABCB1 inhibitor (elacridar) or ABCG2 inhibitor (Ko145) divided by the efflux ratio in the presence of the inhibitor.

[c] Unionization efficiency (λ) is the ratio of unionized form to total drug (the sum of unionized and ionized forms), where the unionized-to-ionized ratio is calculated based on Henderson-Hasselbalch equation: $Log_{10}\frac{base\ (or\ unionized)}{acid\ (ionized)} = pH - PKa$

[d] Intrinsic permeability is the transcellular permeability of the unbound and unionized drug, estimated as the mean $P_{app,A-B}$ normalized by λ.

Data are expressed as the mean ± standard deviation from at least 3 independent experiments (with duplicates in each experiment).

Table 3

PBPK model-predicted unbound drug exposure in the plasma, normal brain, cranial CSF, and spinal CSF at the steady-state following the standard or modified dosing regimens[a]

	Ribociclib		Palbociclib		Abemaciclib	
	Standard (600 mg QD, 21 days)	**Alternative (900 mg QD, 21 days)**	**Standard (125 mg QD, 21 days)**	**Alternative (187 mg QD, 21 days)**	**Standard (150 mg BID, 28 days)**	**Alternative (300 mg QD, 28 days)**
Plasma						
$T_{ss,max}$ (h)	1.32	1.32	3.84	3.84	2.91	3.84
$C_{ss,max}$ (μmol/L)	0.298	0.448	0.038	0.057	0.055	0.062
$C_{ss,min}$ (μmol/L)	0.092	0.139	0.022	0.033	0.045	0.040
$C_{ss,ave}$ (μmol/L)	0.176	0.264	0.029	0.044	0.050	0.050
AUC_{24h} (μmol/L*h)	4.291	6.440	0.779	1.167	1.683	1.326
Brain						
$T_{ss,max}$ (h)	3.84	3.84	3.84	3.84	6.27	10.56
$C_{ss,max}$ (μmol/L)	0.039	0.059	0.005	0.007	0.052	0.053
$C_{ss,min}$ (μmol/L)	0.014	0.020	0.003	0.004	0.051	0.050
$C_{ss,ave}$ (μmol/L)	0.024	0.036	0.004	0.005	0.052	0.052
AUC_{24h} (μmol/L*h)	0.624	0.935	0.096	0.143	1.746	1.391
Brain $K_{p,uu}$ [b]	0.14	0.14	0.12	0.12	1.04	1.05
TER for CDK4[c]	2.4	3.6	0.36	0.45	26	26
TER for CDK6[c]	0.62	0.92	0.27	0.33	5.2	5.2
Cranial CSF						
$T_{ss,max}$ (h)	1.32	1.32	3.84	3.84	6.27	10.56
$C_{ss,max}$ (μmol/L)	0.475	0.713	0.068	0.102	0.039	0.040
$C_{ss,min}$ (μmol/L)	0.149	0.223	0.038	0.058	0.038	0.036
$C_{ss,ave}$ (μmol/L)	0.281	0.421	0.052	0.078	0.038	0.038
AUC_{24h} (μmol/L*h)	6.890	10.33	1.385	2.078	1.311	1.045
CSF $K_{p,uu}$ [d]	1.60	1.60	1.78	1.78	0.78	0.79
Spinal CSF						
$T_{ss,max}$ (h)	3.84	3.84	6.36	6.36	6.27	10.56
$C_{ss,max}$ (μmol/L)	0.404	0.606	0.063	0.094	0.039	0.039
$C_{ss,min}$ (μmol/L)	0.159	0.238	0.040	0.060	0.038	0.037
$C_{ss,ave}$ (μmol/L)	0.263	0.394	0.051	0.076	0.038	0.038
AUC_{24h} (μmol/L*h)	6.742	10.11	1.379	2.069	1.293	1.030
CSF $K_{p,uu}$ [d]	1.57	1.57	1.77	1.77	0.77	0.78

[a] Simulations of 10 trials with 10 subjects in each trial were performed in the Simcyp cancer patient population. Data are presented as the population mean values.

[b] Brain $K_{p,uu}$ is estimated as the AUC_{24h} ratio of unbound brain to unbound plasma at the steady-state.

[c] TER (target engagement ratio) is calculated as the ratio of the average steady-state unbound brain concentrations to the *in vitro* IC_{50} for inhibiting CDK4/6 enzymes.

[d] CSF $K_{p,uu}$ is estimated as the AUC_{24h} ratio of CSF to unbound plasma at the steady-state.

Abbreviations: $C_{ss,max}$, maximum steady-state concentration; $C_{ss,min}$, trough steady-state concentration; $C_{ss,ave}$, average steady-state concentration; AUC_{24h}, area under the concentration time curve during 24 h at the steady-state.